6

Field Test

… in which a relay controlled active load damps oscillations of the generator in a small hydro power station.

A field test at a hydro power plant of Sydkraft AB was arranged to gain experience of load control damping and the associated signal processing in a real system. Whereas this chapter focuses on the control aspects, the signal processing is outlined more in detail in [Akke 1997]. A more complete collection of measurement results is found in [Akke 1996].

On-off control was chosen as it was thought to be straightforward to implement and use. The simulations in Chapter 5 give qualitative understanding of on-off control and the associated problems such as limit cycles. Chapter 5 also demonstrates how the nonlinear system can be analyzed and shows how limit cycles can be avoided. Estimated mode frequency as described in Section 4.5 is used as input to the controller. This signal is practical since it is based on local measurements of electrical signals. With appropriate parameters of the estimator, it produces a signal that closely agrees with the angular velocity of the machine rotor, which was used in Chapter 5.

The field test situation is extremely different from that in the laboratory. The time is very limited – in this case to less than three hours – and the effect of mistakes can be considerably more serious. The control setup was therefore first tested in the laboratory. This provided experience of handling the equipment, that proved useful during the experiment.

Section 6.1 summarizes the characteristics of the power system used for the test. Section 6.2 deals with the signal processing required for the estimation of the mode frequency. The implementation of the control system is treated in Section 6.3. After a brief presentation of the simulation model, the problems associated with obtaining system parameters are discussed in Section 6.4. Section 6.5 shows the results of the experiments along with simulations and finally Section 6.6 concludes the results.

6.1 Power System

When going through the power stations of Sydkraft AB, the hydro power plant of Fig. 6.1 was identified as suitable for damping experiments in several reasons. As the rating of the controlled load should be in reasonable proportion to that of the generator, the machine rating of only 0.9 MW is attractive. Improved damping is better perceived if the inherent damping of the system is low. The lack of damper windings and the fact that the machines can be weakly connected to a strong network indicate that low damping can be arranged.

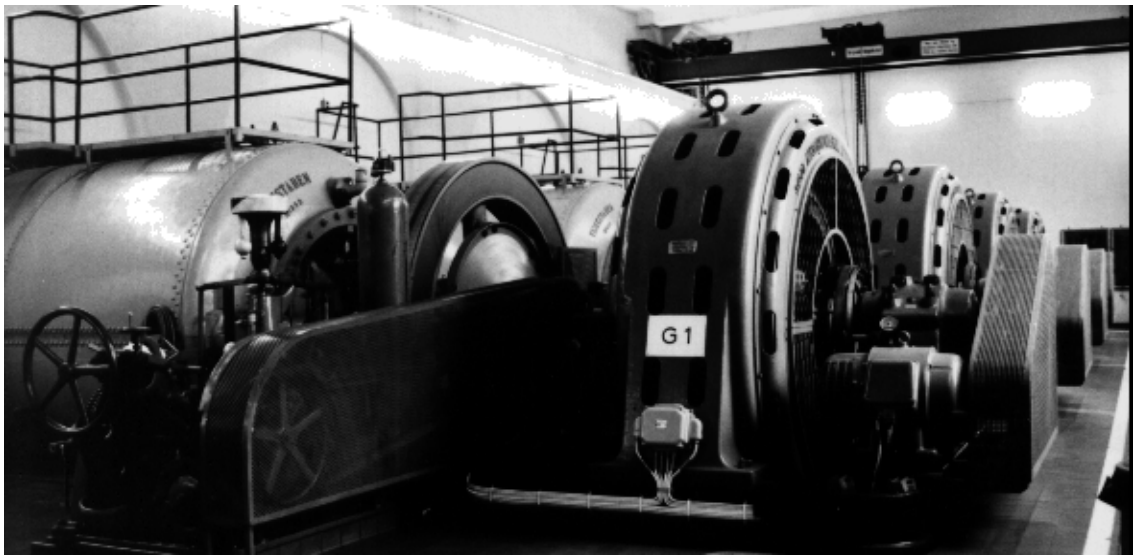

Fig. 6.1 Interior view of the power station with four generating units from 1906.

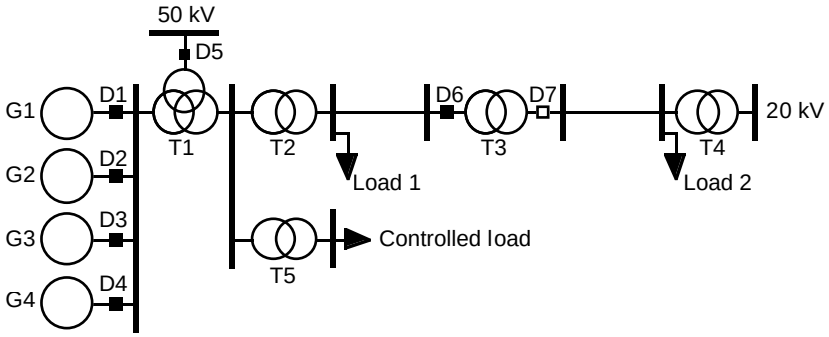

Fig. 6.2 One-line diagram of the test system during normal operation Note that the transformer T3 is not loaded as the disconnector D7 is open.

Fig. 6.2 shows the normal network state of the system that includes two distribution areas. The generators and one distribution area (Load 1) are connected to a 50 kV system via a three winding transformer. The other distribution area (Load 2) is fed from a 20 kV system. The transformer T3 between the two load areas is not loaded.

By opening disconnector D5 and closing D7, Load 1 can be fed from the 20 kV system via transformer T3. This power system configuration is used during the damping experiments. Synchronizing a generator to this network practically results in a single machine infinite bus system, as seen in Fig. 6.3. Its key parameters are given in Appendix A.

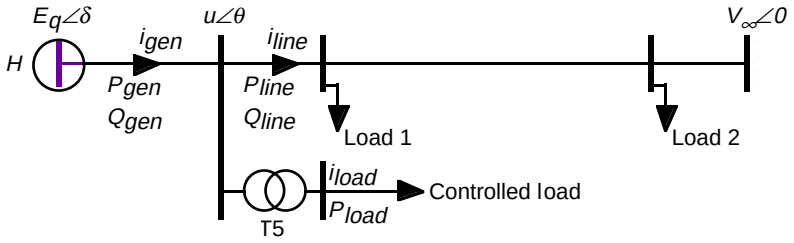

Fig. 6.3 Simplified one-line diagram of the test system during the experiment.

The rating of T3 is small, which permits only one unit of the power plant to be in operation. The fairly large inertia and low rating of the generating unit together with its weak connection to the strong 20 kV system, are prerequisites for low electro-mechanical mode damping.

In the end of September 1996, when the experiment took place, Load 1 exceeded the rating of the transformer T3. Furthermore D5 must be opened before D7 is closed, which causes inconvenience for customers in distribution area 1. Taking this together, the described network state could not be arranged for more than a few hours at one occasion. The limited access to the test system prevented all parameter identification tests, except a load rejection test, from being performed in advance.

6.2 Signal Processing

The signal processing can be divided into three stages: Starting out from single-phase measurements of voltage and currents, active and reactive power is first computed. Next the mode angle is computed and filtered to yield mode frequency. This is finally used for the switching decisions of the relay, that controls the load via thyristor switches. In this section, mode frequency estimation based on active and reactive power is described followed by the procedure for obtaining these signals from the measurements. More details can be found in [Akke 1997].

Mode Frequency Estimation

The mode angle estimation described in Section 4.5, has been applied to the single machine infinite bus system. The bus voltage u in Fig. 6.3 is measured and has the phase angle θ. By using (4.10), δ-θ can be estimated from P_{gen}, Q_{gen} and u, and similarly θ can be determined from P_{line}, Q_{line}

and u. Adding δ-θ and θ now simply gives the machine angle δ relative to the infinite bus. The deviation in rotor angular velocity from the nominal value $\Delta\omega$ is finally obtained by taking the time derivative of δ. As seen in Fig. 6.4, $\Delta\omega$ is sent through a smoothing filter before being used by the relay controller.

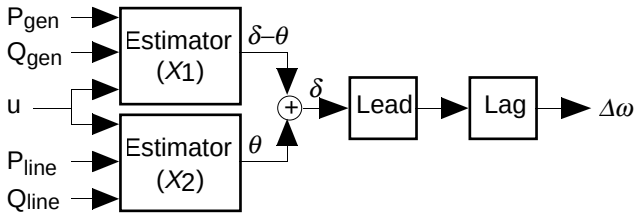

Fig. 6.4 Signal path from active and reactive power to estimate of $\Delta\omega$.

X_1 and X_2 are the only parameters of the estimators. They are set to the reactances seen from the bus where u is measured to the internal bus of the generator (x_q) and to the infinite bus respectively. In the case of X_2 this is a simplification as line resistance has been skipped. Furthermore Loads 1 and 2 are ignored, which is valid if they can be considered constant. This will cause an offset in the θ estimate, but will not affect the $\Delta\omega$ estimate. An alternative is to assume that the loads behave as impedances and merge them into the impedance symbolized by X_2. The former choice is however preferred as it is simpler.

If X_1 and X_2 are not matched to each other, switching of the load gives rise to step changes in δ and consequently spikes in $\Delta\omega$. While a too large X_1 has no effect, a too small X_1 will cause spurious relay switchings. The presence and magnitude of spikes is thus a simple measure of how well the relative values of X_1 and X_2 are chosen. Their absolute values can not be checked in a similar way.

Filtering

The estimator treated above is based on active and reactive power, even if it could use voltage and currents directly. The choice is motivated by the important fact that the computed values of active and reactive power can be checked against panel meters in the control room. This gives a verification that the measurements are correct both regarding phase and magnitude.

The block diagram for how active and reactive power are computed is given in Fig. 6.5. Note that load current is measured instead of line current as it simplifies the measurement setup. For the same reason the generator bus voltage replaces the voltage at the bus between T1 and T2. These voltages are practically equal as the reactance of transformer T1 is small.

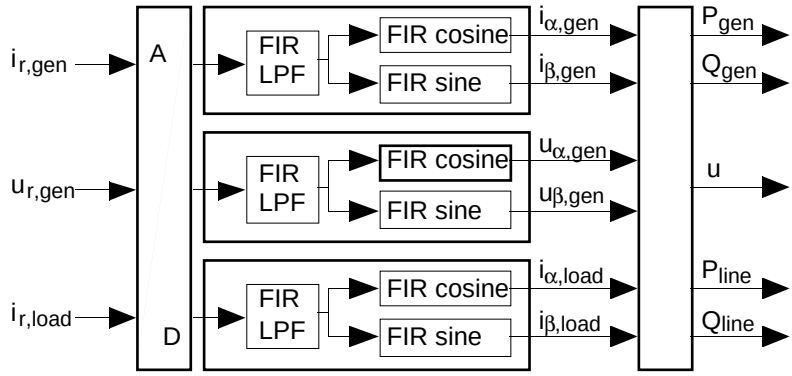

Fig. 6.5 Signal paths from sensors to active and reactive power.

As symmetric conditions are assumed, only single-phase measurements are used of stator current, stator phase voltage and load current respectively. The sensor signals are sampled at 1 kHz and sent through a FIR lowpass filter (20 taps, Hamming window) with a cross over frequency of 100 Hz. In sine and cosine filters each signal is decomposed into two components, α and β, that are orthogonal in phase. It is shown in [Moore et al 1994], that the magnitude response of the sine and cosine filters has an error of ± 1.5 %, if the frequency deviates from the nominal value 50 Hz by 1 Hz. As the error is small and 1 Hz deviation is rather large, the problem is ignored.

Active and reactive power are then obtained as,

$$\begin{cases} P_{gen} = i_{\alpha,gen}u_{\alpha,gen} + i_{\beta,gen}u_{\beta,gen} \\ Q_{gen} = i_{\alpha,gen}u_{\beta,gen} - i_{\beta,gen}u_{\alpha,gen} \end{cases} \tag{6.1}$$

$$\begin{cases} P_{load} = i_{\alpha,load}u_{\alpha,gen} + i_{\beta,load}u_{\beta,gen} \\ Q_{load} = 0 \end{cases} \tag{6.2}$$

The active and reactive power fed into T2, denoted P_{line} and Q_{line} in Fig. 6.4, are finally computed as,

$$\begin{cases} P_{line} = P_{gen} - P_{load} \\ Q_{line} = Q_{gen} \end{cases} \tag{6.3}$$

The reason for going via the load active power, is that the load current was easier to access for measurements.

6.3 Implementation

The computer hardware used for the implementation of the control system consists of a Apple Macintosh IIci housing a DSP (Digital Signal Processor) board [NB-DSP2300/2305] with a TMS320C30 and a general

input/output board MIO-16 both from National Instruments [NB-MIO-16]. The floating point DSP executes all filters and estimators in Fig. 6.6.

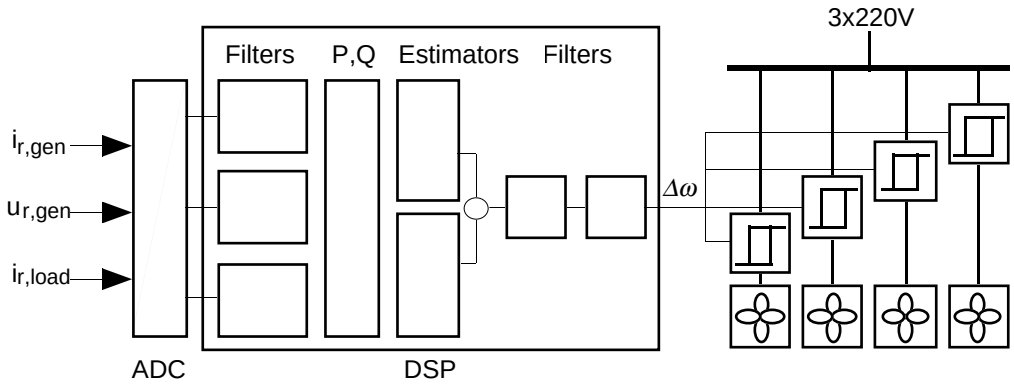

Fig. 6.6 Block diagram of the control system with AD conversion, signal processing and heating fans controlled by relay controlled thyristor switches.

The DSP communicates with a graphical user interface in LabVIEW [LabVIEW] running on the host computer. The user interface shown in Fig. 6.7, makes it possible to change parameters, select modes of operation and to monitor measurements during execution of the control program.

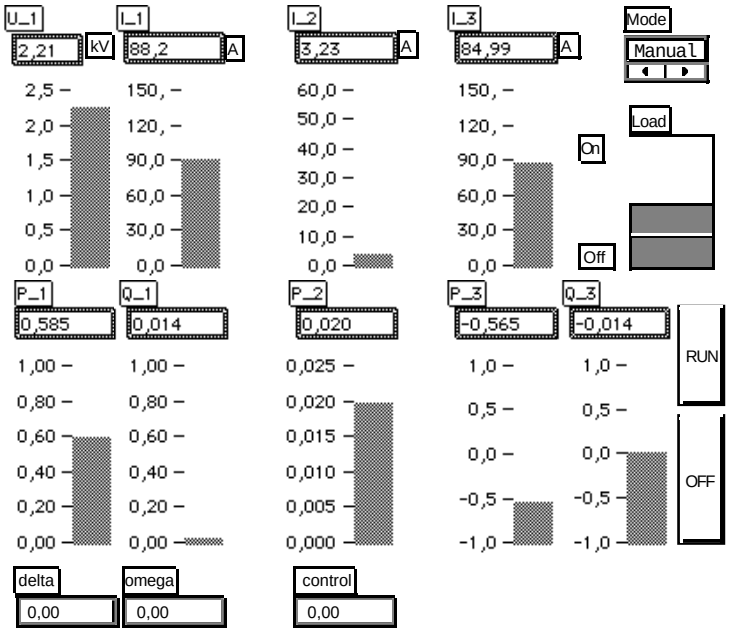

Fig. 6.7 Graphical user interface in LabVIEW with numerical and graphical indicators together with pushbuttons (far right). 6

Fig. 6.8 shows the computers for data logging, control and supervision as they were arranged in the control room of the power station.

Fig. 6.8 Instruments and computers for control, monitoring and data logging.

Fig. 6.9 The controlled active load consisting of four 5 kW heating fans.

The active load consists of four 5 kW heating fans as seen in Fig. 6.9. They are operated with commercially available three-phase thyristor switches mounted in the box shown in Fig. 6.10. The switches are controlled by individual level detectors with selectable levels $\Delta\omega_{on}$ and $\Delta\omega_{off}$ (see Chapter 5) for turning on and off. As the levels are manually selected with a limited accuracy, the switching instants of the fans will differ. An alternative would be to let the DSP take care of the switching decision. This preferable solution would guarantee simultaneous switching, but was not implemented at the time of the field test.

Instead of using the $\Delta\omega$ estimate, the relays can be connected to a signal generator (seen on top of the oscilloscope in Fig. 6.8), which simplifies the creation of a load switching sequence with a certain frequency. A third source for relay control is a manual push-button located on the front panel of the user interface together with the switch for relay control source selection.

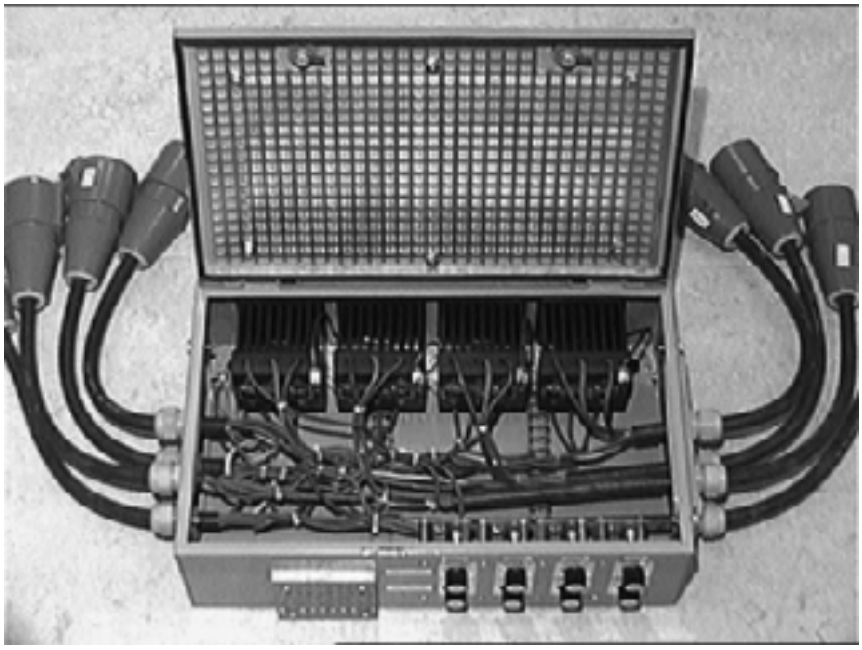

Fig. 6.10 The three-phase thyristor switches are mounted in a box with length 50 cm.

6.4 Simulation Model

A successfully calibrated simulation model is very helpful for the analysis of measurements, as it provides a minimum description of the essential system characteristics. This is particularly valuable when control is based on state estimates, since the controller uses a subsystem model. The agreement between estimate and non-accessible quantity can then readily be studied in the simulation model.

Component Models

The generators have salient pole rotors with no damper windings. The DC exciters have rheostats that are manually controlled. The turbines can be controlled by flyball governors (see Fig. 6.1) for constant frequency, but are normally set for constant power. The simulation model of the system in Fig. 6.3 therefore uses the third order synchronous generator model of EUROSTAG. Its mechanical power and field voltage are set to be constant. The distribution areas are represented by voltage-independent active loads.

Lines, cables and transformers are modelled using standard π-links and the 20 kV bus is made an infinite bus.

Parameters

Generator parameters that quantify dynamic performance typically require special tests in order to be identified explicitly, as they are very difficult to determine during normal operation. An example is the load rejection test, that was carried out to determine the inertia constant H. The generator is then electrically disconnected at a low turbine power level with the governor set for constant frequency. The initial acceleration, before governor action shuts down the turbine, together with the known turbine power gives H.

Tests to identify machine reactances could not be performed before the feedback experiment. Instead the excitation test of Section 6.5 serves as dynamic identification experiment. The calibration of the simulation model is done in two stages, treated in more detail in Section 6.5: the first part aims at agreement between simulated and measured generator output power and the second deals with the estimator tuning.

The values of X_1 and X_2 used during the experiment, had to be based on available data of the generator, transformers, lines and cables read from rating plates, manufacturer data sheets and maps. It is important to realize that, if their relative magnitudes are correct, modest changes of X_1 and X_2 only yield a rescaling of the $\Delta\omega$ estimate. This will not alter the qualitative behaviour of the control system and the results of the experiment.

6.5 Experiments

All experiments of the field test except the load rejection test, were performed during three hours between two and five o'clock in the morning. The same experiments have been simulated afterwards using the measurements from one experiment for calibration of the simulation model. To facilitate comparisons, the results of measurements and simulations are presented together.

Synchronizing the Machine to the Grid

When the network state of Fig. 6.3 had been arranged, the generator was synchronized to the network.

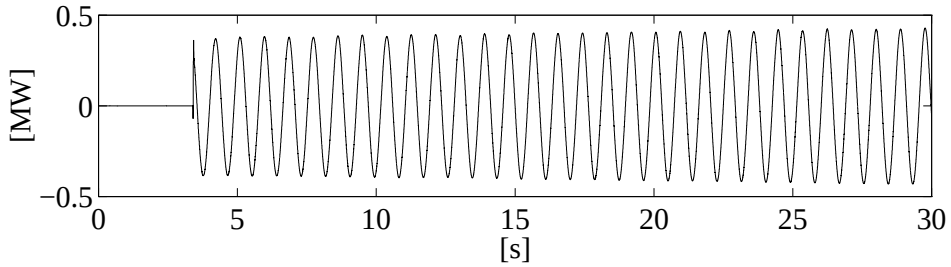

Fig. 6.11 Measurement of generator active power following synchronization.

Fig. 6.11 shows the instant when the machine is connected to the network, followed by an oscillation with slowly increasing amplitude. The damping is thus not only low, but negative. According to [Kundur 1994] p 752 this happens "when a hydraulic generator without damper windings is operating at light load and is connected by a line of relatively high resistance to reactance ratio to a large system", which is exactly the case here. Using the *K* constants in [de Mello and Concordia 1969] the situation above makes K_4 negative. K_4 is the "demagnetizing effect of a change in rotor angle" and becomes negative when a factor of it is negative,

$$\left(x_q + x_{line}\right)\sin\delta - \left(R_a + r_{line}\right)\cos\delta < 0 \qquad (6.4)$$

where $r_{line}+jx_{line}$ is the line impedance while R_a,x_q and δ are the armature resistance, the q-axis reactance and the load angle of the machine respectively.

With an unstable synchronous generator running, the damping system was engaged for the first time. The oscillations amplitude started to decrease indicating that, with only rough tuning of the three parameters X_1, X_2 and $\Delta\omega_{on}$, the damper was actually functioning. Unfortunately the event was not recorded. After disconnection of the machine, the procedure with synchronization and activation of the damper was repeated, giving the results shown on the cover page.

Excitation of Oscillations

Having selected 50 % of rated output a operating point, the instability of the machine disappears as predicted by (6.4). The swing frequency of the system is now determined through repeated switching of the controlled load. By using the signal generator, different frequencies can conveniently be tested. Hitting the swing frequency manifests itself as an oscillation with increasing amplitude in most variables as seen in Fig. 6.12.

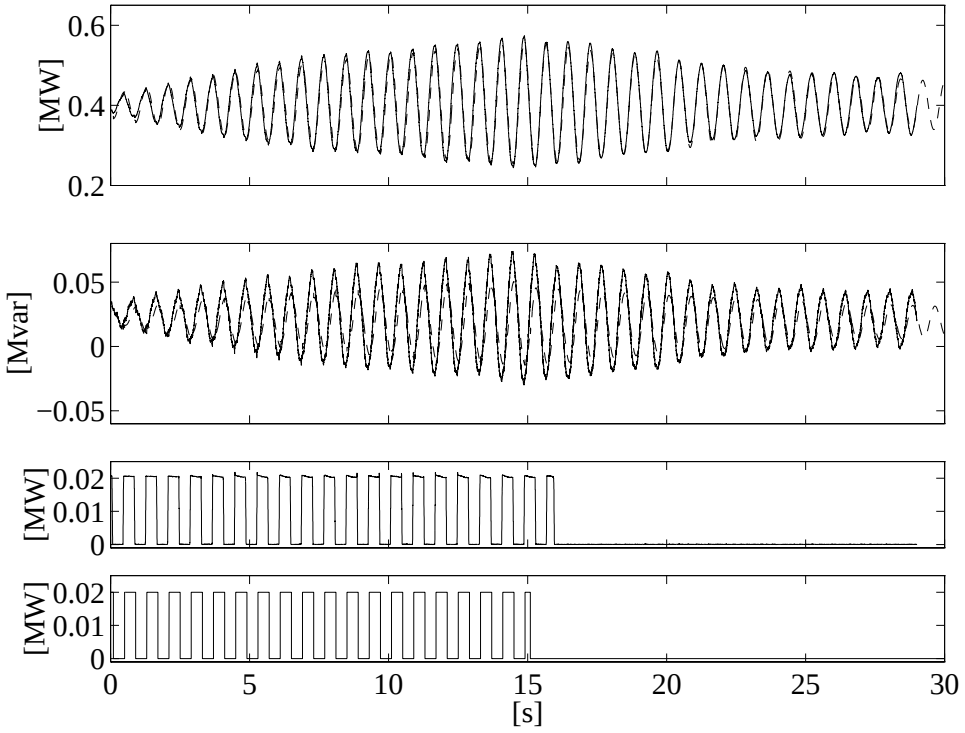

Fig. 6.12 Excitation with signal generator: P_{gen}(t) (top), Q_{gen}(t) (middle) from experiment (solid lines) and simulation (dashed lines). The two lower graphs show P_L(t) from experiment and simulation (bottom).

While seeming simple, this experiment is extremely valuable: It demonstrates how an oscillation with appreciable amplitude can be evoked. This is a very important prerequisite for evaluating the performance of the damping controller. Furthermore, by studying the behaviour after the load switching has ceased in Fig. 6.12, the damping at the selected operating point can be determined.

The load switching excites the system dynamics better than normal operation. The measurements of Fig. 6.12 can therefore be used for calibration of the simulation model as follows: the frequency of the free oscillation is adjusted with x_q. Subsequently x'_d is adjusted so that a certain portion of the load power is taken from the machine. Finally the correct damping is set with D. The dashed lines in Fig. 6.12 are the results from simulations using the calibrated model, which agree well with the measurements. An exception is the amplitude of the Q_{gen} which is 50 % too small. At this operating point this is no problem as changing Q_{gen} by a factor of two affects the estimate of δ-θ by less 0.5°.

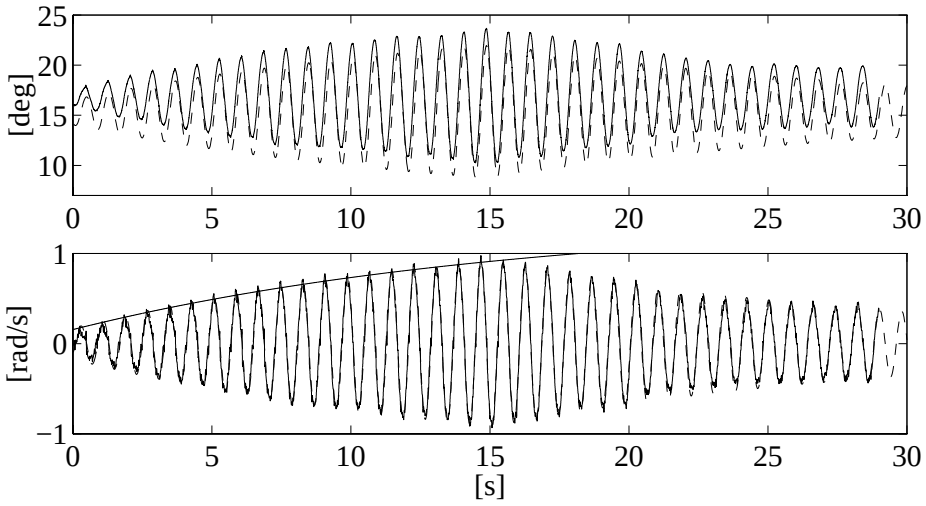

Fig. 6.13 Excitation with signal generator: Estimates of $\Delta\omega$(t) and $\delta(t)$ from experiment (solid lines) and simulation (dashed lines). The fitted exponential is used to demonstrate relay parameter selection. Its time constant is 16 s and it asymptotically approaches 1.4 rad/s.

As the $\Delta\omega$ estimate from the experiment in Fig. 6.13 exhibits no spikes, there was no reason to alter the reactance values during the experiment. From Fig. 6.13 it is evident that the estimates of $\Delta\omega$ and δ from the experiment agree well with the simulated $\Delta\omega$ and δ. This indicates that the estimator parameters were reasonable even if they were based on another value of x_q than that arrived at during the calibration.

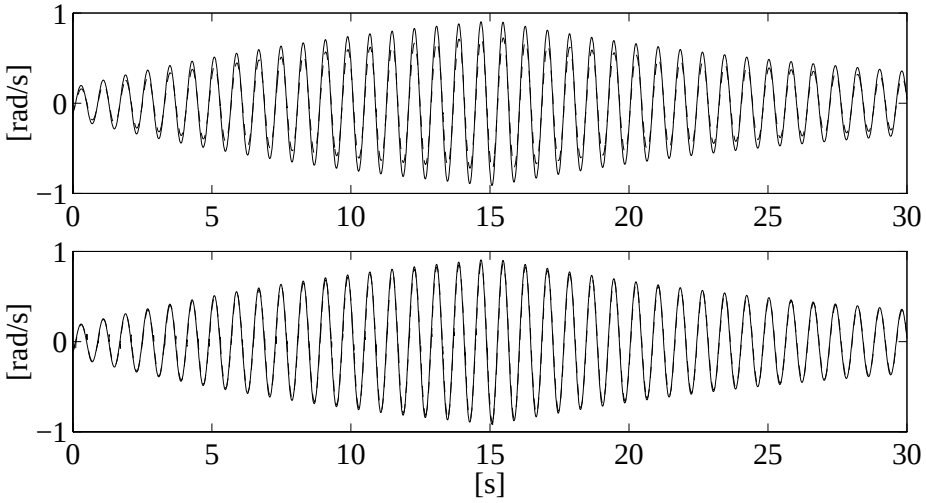

Fig. 6.14 Excitation with signal generator: True (solid lines) and estimated values of $\Delta\omega(t)$ (dashed lines) from the simulation using X_1 and X_2 from the experiment (top) and after calibration (bottom).

The upper part of Fig. 6.14 shows that the true $\Delta\omega$ in the simulation and its estimate are fairly similar using X_1 from the experiment. By adjusting X_1 to

the new value of x_q perfect agreement can be achieved as seen in the lower part of Fig. 6.14.

As described in Section 5.3, the minimum value of the relay parameter $\Delta\omega_{on}$ can be obtained from the excitation experiment. The fitted exponential of Fig. 6.13 has a time constant of 16 s and asymptotically approaches 1.4 rad/s. The load is switched with a frequency of 1.25 Hz. By inserting this into (5.7) the minimum value of $\Delta\omega_{on}$ in order to avoid a limit cycle can be determined to 0.035 rad/s.

Damping of Oscillations

Having checked the estimator, the damping controller can now be tested. An oscillation is then evoked, using the same technique as above, but after excitation ceases, the active damper is engaged. This is done for different values of $\Delta\omega_{on}$: 1, 1/4, 1/6 and 1/8 rad/s. Fig. 6.15 shows the results for $\Delta\omega_{on}$=0.17 rad/s. Although the excitation stops earlier than in Figs 6.12 and 6.13, the added damping effect is evident.

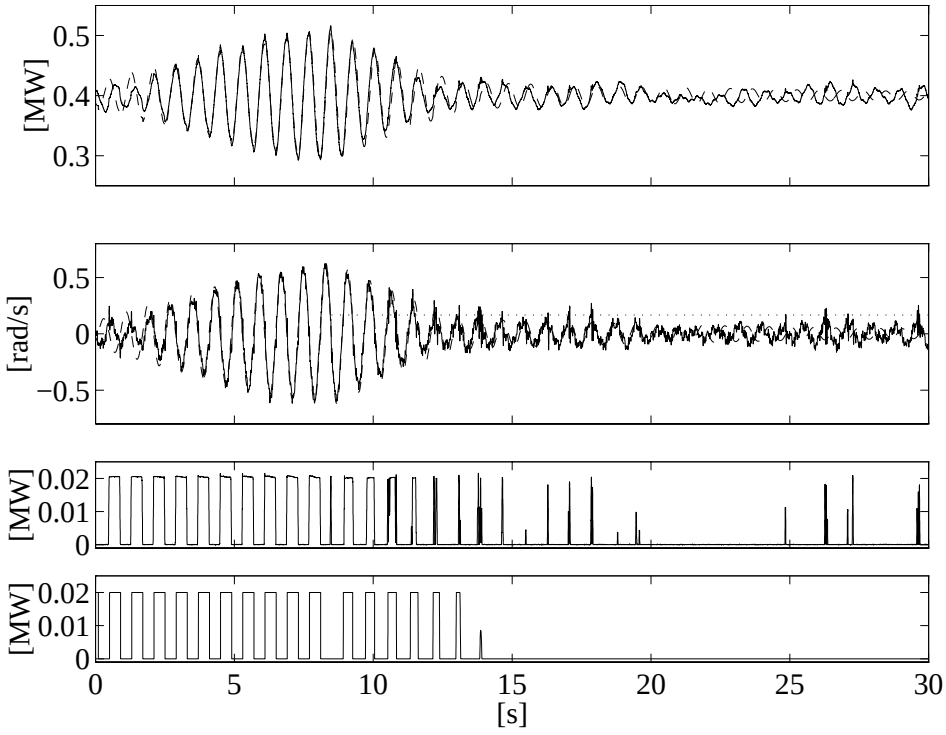

Fig. 6.15 Signal generator excitation until time 8.5 s followed by relay damping, $\Delta\omega_{on}$ =0.17 rad/s (dotted line): P_e(t) (top) and estimate of $\Delta\omega(t)$ (middle) from experiment (solid) and simulation (dashed). The two lower graphs show P_L(t) from experiment and simulation (bottom).

Whereas the signal path of the relay in Chapter 5 was free from delays, the implementation used for the experiment includes several filters. Due to the

resulting delay the load will be switched on at a higher $\Delta\omega$ than $\Delta\omega_{on}$ and off at a level less than $\Delta\omega_{off}$. While $\Delta\omega_{off}$ was set to zero in Chapter 5, a value equal to $\Delta\omega_{on}$ was used for the experiments. The switching is then practically delayed until $\Delta\omega$ passes zero, which is the desired instant.

Other values of $\Delta\omega_{on}$ give similar results: the oscillation is damped until the amplitude of $\Delta\omega$ is less than $\Delta\omega_{on}$. Some differences are found: as $\Delta\omega_{on}$ is decreased, the time during which the load is connected will increase. This causes the oscillation to be damped faster the smaller $\Delta\omega_{on}$ is. Furthermore, as the system does not settle down entirely, the damping controller is more active during steady state for small values of $\Delta\omega_{on}$. This is exemplified by Fig. 6.16, which shows damping performance for $\Delta\omega_{on}$=0.125 rad/s.

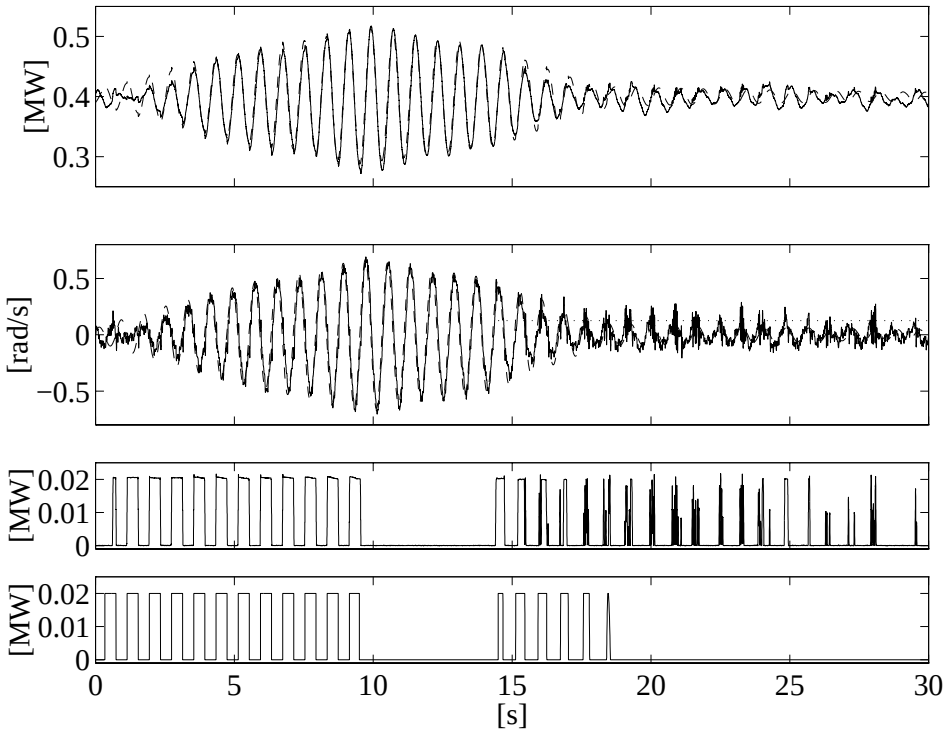

Fig. 6.16 Signal generator excitation until time 10 s followed a short interval of natural damping and relay damping with $\Delta\omega_{on}$ =0.125 rad/s (dotted line): P_e(t) (top) and estimate of $\Delta\omega(t)$ (middle) from experiment (solid) and simulation (dashed). The two lower graphs show P_L(t) from experiment and simulation (bottom).

As this steady state activity is judged too high, lower values of $\Delta\omega_{on}$ were not tested. $\Delta\omega_{on}$ was thus never close to values that would give a limit cycle.

6.6 Conclusions

The field test clearly shows that an active load can be controlled to damp power oscillations. It also demonstrates that a load that draws only 5 % of the power supplied by the generator equally well can both excite considerable oscillations and damp them. This agrees well with the examples given in Chapter 5. The same behaviour can be reproduced, even quantitatively, with the calibrated EUROSTAG simulation model. The use of estimated rotor angular velocity is proved to be practically viable.

It is natural to compare the damper of the field test with a PSS (Power System Stabilizer) as they solve the same problem and as PSSs exist, that use the same estimated signal for feedback [Kundur 1994]. A PSS affects the oscillating active power indirectly, by manipulating the field voltage of the generator, which in turn changes the terminal voltage. This changes the power output from the generator and the active power drawn by local loads. The PSS contains circuitry that, when properly tuned, compensates for the dynamics between its control input and the active power output of the machine. Controlling active power as in the field test is more direct, which eliminates much of the tuning work, which is the main disadvantage of a PSS. The damper of the field test only required X_1 and X_2 to be chosen so that the estimate of $\Delta\omega$ is continuous. The relay parameter $\Delta\omega_{on}$ is simply set so that the oscillation is sufficiently small. In comparison to a PSS, this tuning is very straightforward and easily understandable.

The mode frequency estimation is easy to implement in radial networks, such as distribution networks. In distribution networks loads are electrically close to the machines, which makes them effective for load control damping. The chosen test system thus represents a suitable location of a load control damper.

The field test has given practical experience regarding system knowledge and operational practice. This is an invaluable complement to simulations and written material, that are usually the only sources of knowledge in power engineering research.